nature nanotechnology

ARTICLES

PUBLISHED ONLINE: 21 APRIL 2013 | DOI: 10.1038/NNANO.2013.66

Dynamic switching of the spin circulation in tapered magnetic nanodisks

V. Uhlíř[1,2]*, M. Urbánek[2,3], L. Hladík[3], J. Spousta[2,3], M-Y. Im[4], P. Fischer[4], N. Eibagi[1], J. J. Kan[1], E. E. Fullerton[1] and T. Šikola[2,3]

Magnetic vortices are characterized by the sense of in-plane magnetization circulation and by the polarity of the vortex core. With each having two possible states, there are four possible stable magnetization configurations that can be utilized for a multibit memory cell. Dynamic control of vortex core polarity has been demonstrated using both alternating and pulsed magnetic fields and currents. Here, we show controlled dynamic switching of spin circulation in vortices using nanosecond field pulses by imaging the process with full-field soft X-ray transmission microscopy. The dynamic reversal process is controlled by far-from-equilibrium gyrotropic precession of the vortex core, and the reversal is achieved at significantly reduced field amplitudes when compared with static switching. We further show that both the field pulse amplitude and duration required for efficient circulation reversal can be controlled by appropriate selection of the disk geometry.

Magnetic vortices are the curling magnetization structures that represent the lowest energy state in submicrometre-sized magnetic disks or polygons[1] where the flux closure character is exchange-compensated by the vortex core in the disk centre[2,3]. The vortex state is characterized by the circulation of the magnetization in the plane of the disk, either anticlockwise or clockwise ($c = +1$ or -1), and the polarity of the core, which points either up or down ($p = +1$ or -1), perpendicular to the disk plane. ('Spin circulation' directly refers to the binary character of the flux-closing magnetization state, whereas the term 'vorticity', sometimes used in the literature, is a continuous measure of the total magnetization curl and is better suited to describe general magnetization states, such as C-states.) The combination of circulation and polarity defines chirality (handedness), that is, whether it is a right-handed ($cp = +1$) or left-handed ($cp = -1$) vortex.

When excited by a fast-rising magnetic field or spin-polarized current, vortices exhibit a rich variety of fundamental dynamic behaviours that are inherent to chiral structures[4–12]. Generally, the magnetization distribution of a vortex is an example of a magnetic topological soliton[13] and features low-frequency precessional modes[5,8] associated with the translational motion of the core. The precessional mode has been the subject of considerable interest, with applications in oscillators[11,12] and resonant amplification of gyrotropic precession for low-field[14,15] or low-current[16] excitations.

Because of their multiple stable ground states, vortices have also been studied as potential multibit memory cells[17–19]. This application requires independent control of both the circulation and the polarity. The polarity can be reversed by applying a static out-of-plane magnetic field, although its magnitude needs to be quite large, on the order of 0.5–1.0 T (ref. 20). However, fast stimuli can lead to much more efficient core polarity switching. Using a magnetic field[14,21,22] or current[16], the vortex core can be driven into gyrotropic precession and the core polarity reversed as soon as the core reaches a critical velocity[16,23,24]. This effect is similar to Walker breakdown in domain-wall motion in nanowires[1,23]. Instability of the core leading to polarity reversal can be also induced by excitation of high-frequency azimuthal spin wave modes using rotating magnetic fields[25]. The mechanism of polarity reversal generally involves the creation and annihilation of a vortex–antivortex pair, followed by the formation of a core with opposite polarity, which can occur in less than 0.1 ns (refs 21,26,27).

The subnanosecond character of vortex polarity switching raises the question of controlling the spin circulation on similar timescales, thus opening a path to selective and independent control of the polarity and circulation. Unlike switching core polarity, controlled switching of spin circulation with magnetic fields requires displacing the vortex core out of the disk and then reforming the vortex with the opposite spin circulation. The core expulsion can be performed by using an in-plane static magnetic field that moves the core to the side of the disk and finally annihilates the vortex when $B_{\text{an-stat}}$ is reached[28]. The sense of magnetization circulation that forms as the field is removed can be controlled either by exploiting an asymmetry in the structure shape[29–31] or in the spatial distribution of the applied magnetic field[32–35]. Symmetry-breaking in vortex creation can also be achieved by interfacial effects, such as exchange biasing[36] or the Dzyaloshinskii–Moriya interaction[37]. Other approaches have been proposed based on spin-transfer torque[38] or dynamic evolution of the C-shaped magnetization states after expelling the vortex core[9]. However, until now, control of spin circulation in magnetic vortices has only been demonstrated experimentally under static conditions.

Here, we show that far-from-equilibrium gyrotropic precession enables dynamic switching of spin circulation and substantially decreases the dynamic annihilation field $B_{\text{an-dyn}}$ compared with static conditions. This annihilation field reduction is analogous to the reduction of switching fields in Stoner–Wohlfarth particles[39] by precessional reversal using fast-rising magnetic field pulses[40]. We further show that the lower bound of the time required for spin circulation switching is set by the gyrotropic eigenfrequency of the vortex core motion, which is defined by the disk geometry[5].

In the present experiments we study permalloy ($Ni_{80}Fe_{20}$) disks of different diameters (250–1,100 nm) and thicknesses (20 and

[1]Center for Magnetic Recording Research, University of California, San Diego, 92093-0401 La Jolla, California, USA, [2]CEITEC BUT, Brno University of Technology, Technická 10, 616 00 Brno, Czech Republic, [3]Institute of Physical Engineering, Brno University of Technology, Technická 2, 616 69 Brno, Czech Republic, [4]Center for X-ray Optics, Lawrence Berkeley National Laboratory, 1 Cyclotron Road, 94720 Berkeley, California, USA. *e-mail: vojtech.uhlir@uh.cz

© 2013 Macmillan Publishers Limited. All rights reserved.

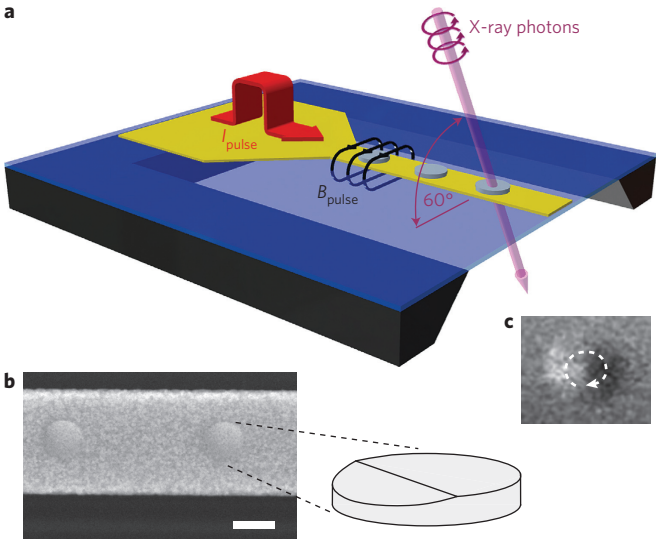

Figure 1 | Sample configuration. a, Schematic of the sample: a nanodisk chain fabricated on top of a 50-nm-thick gold waveguide. An applied positive current I_{pulse} produces an in-plane field B_{pulse} transverse to the stripline. The stripline is fabricated on a 200-nm-thick Si_3N_4 membrane window, which is transparent to the incoming soft X-rays, allowing imaging in transmission geometry. **b**, A scanning electron microscopy (SEM) image showing the detail of a 500-nm-wide and 20-nm-thick disk. The thickness asymmetry at the bottom-left part of the disks is highlighted by the schematic close-up. Scale bar, 500 nm. **c**, Magnetic contrast in the image of a 1,000-nm-wide nanodisk after dividing it with a reference image containing a vortex with the opposite spin circulation. The curl of the magnetization is indicated. The black and white domains represent parallel and antiparallel orientation of the magnetization projected on the incident soft X-ray beam.

30 nm) that are excited by externally applied static magnetic fields or by applying in-plane magnetic field pulses created by current pulses in a waveguide (details of the sample and waveguide are shown in Fig. 1). Magnetization states were imaged with full-field magnetic soft X-ray transmission microscopy (MTXM) at the Advanced Light Source (ALS), BL 6.1.2 (ref. 41; see Methods for details). The presence of the vortex is seen as a black/white contrast across the disk (Fig. 1c).

Figure 2a–c shows the remanent magnetic states of 510-nm-wide and 20-nm-thick disks (referred to as 510/20 disks hereafter) after application of static magnetic fields. Before applying the magnetic fields, the spin circulations in the disks were random (not shown). Figure 2a illustrates the situation after applying a negative field of −90 mT, which is sufficient to saturate the magnetization and expel the vortex core. All disks show identical circulation after removing the field. Upon increasing the field amplitude in the positive direction, there is a threshold above which the circulation in the individual disks begins to switch (Fig. 2b); finally, a positive field of 34 mT results in switching of all the circulations in the opposite direction (Fig. 2c). This indicates a modest distribution in static vortex annihilation field $B_{an\text{-}stat}$ within one sample. Similar images for 250/20 disks are shown in Fig. 2d,e, with $B_{an\text{-}stat} = 51$ mT. The measured values of $B_{an\text{-}stat}$ for different disk geometries are listed in Table 1 and are taken as the field at which 50% of the circulations have switched.

Based on Fig. 2a–e we can conclude that the final circulation is the same in all the disks and depends solely on the sign of the applied magnetic fields (Supplementary Fig. S1). This is a result of a controlled symmetry-breaking in the disks arising from a wedge-like variation in the disk thickness at the disk boundary (Fig. 1b). Note that a small induced uniaxial anisotropy might also be present, but this does not contribute to symmetry-breaking in circulation creation. Although magnetic dipolar interaction between the disks can be neglected when the disks are in a vortex state, it can become significant when the disks reach the monodomain state after vortex annihilation[42,43]. However, this effect cannot provide an explanation for the formation of a uniform spin circulation in the long chain of disks we are studying. Although edge roughness and lithography defects breaking the circular symmetry of the disks could also play a role, the final circulation was the same in all the disks of the chain, even in samples with different disk geometries.

Figure 2f–h shows the remanent magnetic state in 250/20 disks in response to pulsed magnetic fields. Figure 2f shows the initial state set by a static field, and Fig. 2g,h shows the magnetic states after applying 1 ns and 1.5 ns pulsed fields, respectively, to initiate dynamic switching. These images show that control of the final circulation is maintained using pulsed fields, but the dynamic annihilation threshold field ($B_{an\text{-}dyn}$) is only 26 mT (Fig. 2g), which is roughly half $B_{an\text{-}stat}$ (Fig. 2e). Although we see a significant reduction in the switching field with pulsed current, there is a lower limit to the pulse duration

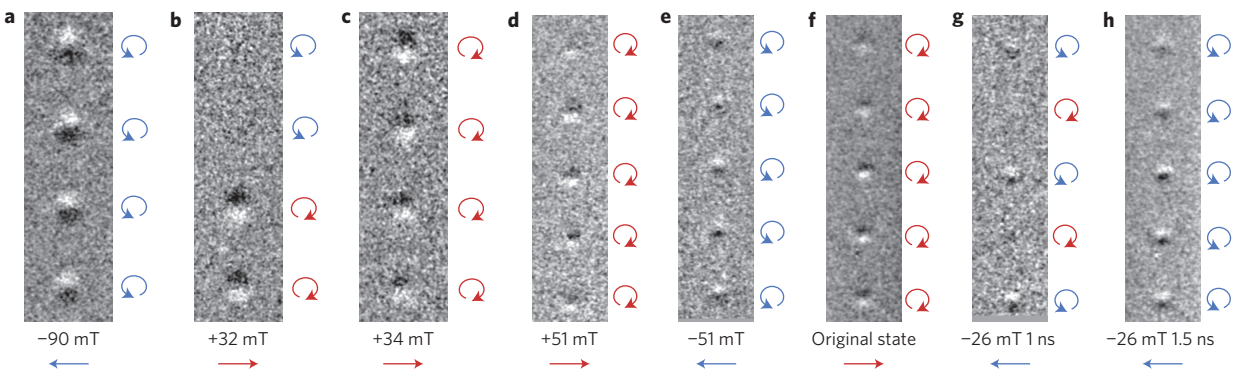

Figure 2 | MTXM images showing the switching of spin circulation in magnetic vortices by static magnetic fields and field pulses. The MTXM images of vortices were taken after application of in-plane magnetic fields. The arrows on the right of each image indicate spin circulation. Arrows and labels below the images show the polarity and magnitude of the applied field, as well as pulse duration where applicable. **a–c**, Switching of spin circulation in 510/20 disks by a static magnetic field. **d**,**e**, Switching of spin circulation in 250/20 disks by a static magnetic field. **f**, Initial magnetization configuration in 250/20 disks before applying magnetic field pulses. **g**,**h**, Final state after applying a 26 mT pulse of 1 ns (**g**) and 1.5 ns (**h**). Each image is divided by a reference image containing all vortices with the original spin circulation, that is, before applying the magnetic field in each case. Only the vortices that have switched circulation therefore show magnetic contrast.

© 2013 Macmillan Publishers Limited. All rights reserved.

Table 1 | Static and dynamic annihilation fields for different disk geometries.

Diameter/thickness (nm)	$B_{an\text{-}stat}$ simulated (mT)	$B_{an\text{-}stat}$ (mT)	$B_{an\text{-}dyn}$ (mT)	$B_{an\text{-}dyn}/B_{an\text{-}stat}$	t_s (ns)
250/20	67	51	26	0.51	0.95
510/20	53	32	14	0.44	1.45
960/20	39	27	13	0.48	2.45
1,000/20	38	29	17	0.59	2.45
1,040/20	37	23	11	0.48	2.75
560/30	66	48	22	0.46	2.75
1,100/30	46	37	20	0.54	3.45

$B_{an\text{-}stat}$, $B_{an\text{-}dyn}$ and switching time t_s, indicating the minimum pulse duration where switching was observed, listed for different disk geometries. The average value of $B_{an\text{-}dyn}/B_{an\text{-}stat}$ is 0.50 ± 0.02 mT.

where switching is not observed or could only be achieved at higher applied fields. In 250/20 disks, the onset of switching was observed for pulses of 1 ns (Fig. 2g) or longer (Fig. 2h). The minimum pulse amplitudes and durations required for circulation switching are summarized in Table 1 and the minimum pulse durations are plotted in Fig. 3b (blue triangles) for 20-nm-thick disks. The significant decrease in field pulse amplitude was observed for different disk geometries (Table 1) with ratios $B_{an\text{-}dyn}/B_{an\text{-}stat}$ varying from 0.44 to 0.59.

Although the details we observe can be reproduced by micromagnetic simulations (as described in the following) the trends directly emerge from analytical models describing vortex dynamics. The magnitude of the static annihilation field can be determined using the rigid-core model[28,44]. It satisfactorily predicts the annihilation fields for a wide range of L/R, where L is the disk thickness and R its radius. A static magnetic field moves the vortex core to a new equilibrium point (Fig. 3c), which is at a distance s from the disk centre, where $s = R\chi B/(\mu_0 M_S)$ (ref. 5, 28; where χ is the static susceptibility of the vortex state, B is the applied magnetic field, and M_S is the spontaneous magnetization of the material). Because of a flux-closing magnetization configuration in vortices, their annihilation requires expelling the vortex core out of the disk, which occurs when $s = R$.

The process of core annihilation is qualitatively different when using pulsed magnetic fields with a rise time much shorter or comparable with the period of the translational vortex eigen-oscillation[5]. Applying such a pulse causes the vortex core to gyrate about an equilibrium point determined by the amplitude of the pulse. The trajectory of the vortex core is approximately circular (Fig. 3d, solid line) if the nonlinearity of χ for $s/R \rightarrow 1$ is neglected. The switching is most efficient when the core is annihilated during the first half-period of the gyration (Fig. 3d). In this regime the influence of damping on the core trajectory can be neglected[5] and the threshold $B_{an\text{-}dyn}$ corresponds to $s = R/2$. In this case, the model predicts $B_{an\text{-}dyn} = B_{an\text{-}stat}/2$, which is close to our experimental observations. Note that the measured $B_{an\text{-}stat}$ values listed in Table 1 include any possible deviations from the expected values due to sample imperfections.

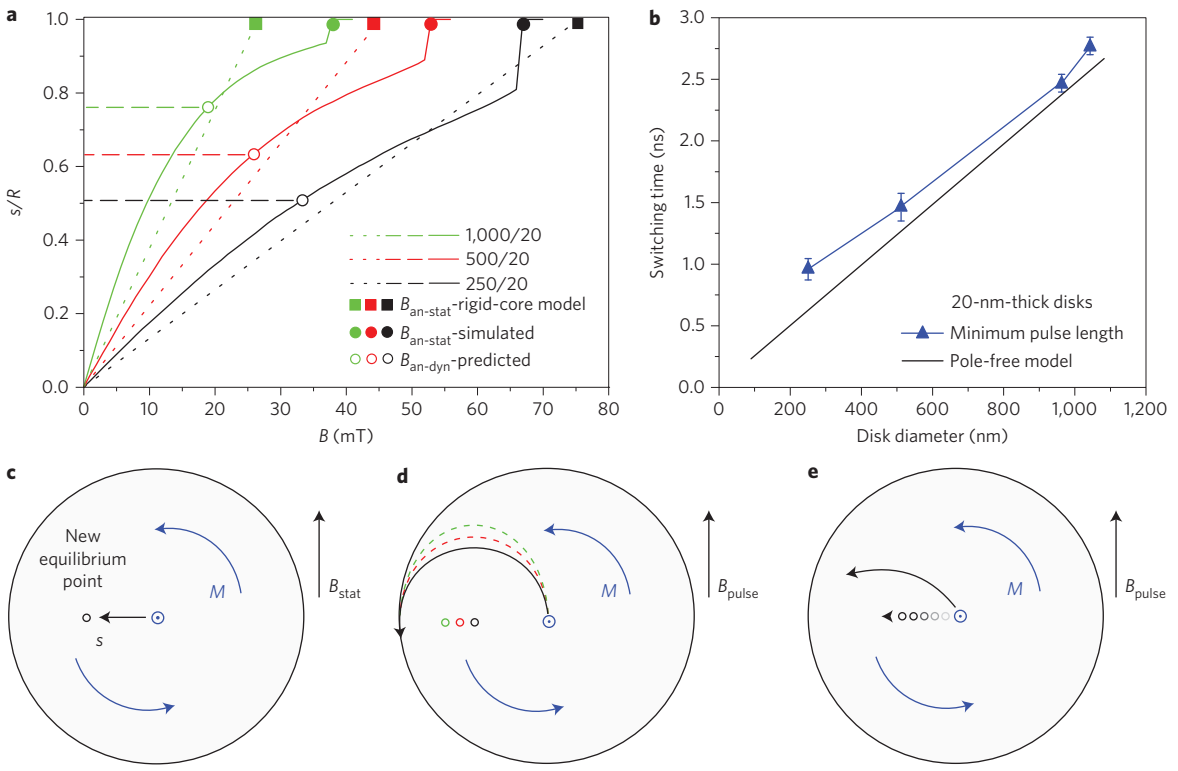

Figure 3 | Conditions for static and dynamic annihilation of the vortex core. a, Solid lines indicate simulated s/R versus B curves for 20-nm-thick disks of different diameters (labelled by diameter/thickness in nm). Full circles indicate simulated $B_{an\text{-}stat}$ fields. Open circles represent approximate $B_{an\text{-}dyn}$ fields corresponding to the values $B_{an\text{-}stat}/2$. Dashed lines are guides to the eye to read the distance of the initial equilibrium point. Dotted lines indicate relative vortex core displacement as a function of B predicted by the rigid-core model. Squares indicate $B_{an\text{-}stat}$ fields predicted by the rigid-core model. **b**, Minimum measured pulse durations needed for spin circulation switching (solid symbols) compared to half-period times calculated using the pole-free model. **c**, Displacement s of the vortex core by a quasi-static magnetic field. **d**, Black line indicates a core trajectory induced by a fast-rising magnetic field assuming a linear static susceptibility. Red and green dashed lines and circles schematically represent the trajectories and the equilibrium points for disks with diameters of 500 nm and 1,000 nm, respectively, with an increasing nonlinearity of static susceptibility. **e**, Effect of a field pulse with rise time comparable to the period of the core eigen-oscillation. The core gyrates about a moving equilibrium point, and therefore follows a cycloidal trajectory.

© 2013 Macmillan Publishers Limited. All rights reserved.

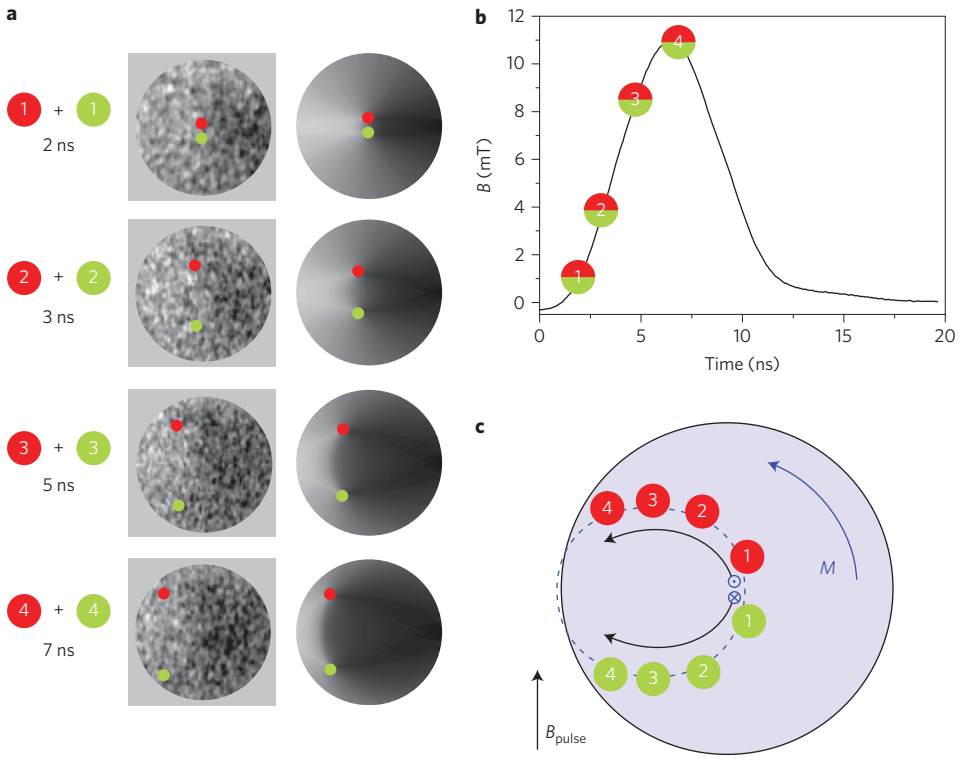

Figure 4 | Temporal evolution of dynamic annihilation of the vortex core. a, Sequence 1–4. Left column: time-resolved MTXM images of the dynamic response of a magnetic vortex in a 1,040/20 disk to the unipolar magnetic field pulse plotted in **b**. Right column: images obtained by a micromagnetic simulation explaining the observed contrast. All images were divided by a reference in the saturated state. The images are a sum of two alternative trajectories for a core polarity up and a core polarity down. Red and green dots mark the approximate positions of the vortex cores with the polarity up and down, respectively. **b**, The points indicated on the pulse time profile represent the instants when the X-ray flashes hit the sample. They are identical for both core polarities (combined numbered tags). **c**, Schematic of the two vortex core trajectories during vortex annihilation.

A more quantitative understanding requires an extension beyond the linear rigid-core model. As the core approaches the disk boundary, the vortex susceptibility falls into the nonlinear regime and a realistic dependence of the vortex core displacement s on applied field B should be taken into account. Figure 3a presents s/R versus B curves that demonstrate vortex annihilation for 20-nm-thick disks calculated using micromagnetic simulations[45] and the rigid-core model. To directly compare these two approaches, the wedge-like disk asymmetry is not included in the simulation. At low applied fields, the initial susceptibility predicted by the rigid-core model (dotted lines) is lower than that obtained by simulations. The linear regime ends at approximately $s = 0.25R$, which is consistent with experimental observations[46].

Beyond this regime, the simulated susceptibility progressively decreases, and for large s/R becomes lower than the susceptibility predicted by the rigid-core model. This nonlinearity is more apparent in the case of disks with larger R. The model overestimates $B_{\text{an-stat}}$ for small disks and underestimates it for large disks (Supplementary Fig. S2). Hence, the equilibrium points corresponding to dynamic annihilation fields, $B_{\text{an-dyn}} = B_{\text{an-stat}}/2$ (Fig. 3a, open circles), are also greater than $0.5R$ for disks with larger R ($\sim 0.65R$ for 500 nm disks and $\sim 0.75R$ for 1,000 nm disks). As a result, the core trajectories become elliptical (Fig. 3d, dashed lines), as has been observed experimentally[46].

Because the threshold dynamic switching occurs for a half-period of the core gyration, the corresponding eigenfrequency ω_0 can be used to estimate the lower limit of the switching time. ω_0 can be approximated by the pole-free model in the linear vortex susceptibility regime[5]. The calculated switching time is shown in Fig. 3b as the black solid line that tracks the experimental values with an offset. This offset is largely a result of the finite rise time of the experimental field pulse ($\sim$0.5 ns; see Methods). Another contribution comes from the fact that the experimental core frequency was found to be lower than predicted for high-aspect-ratio disks[47]. In our case this can be explained both by the effect of edge roughness and the thickness asymmetry that effectively increases χ and decreases ω_0. The model's neglect of core annihilation at the disk boundary has a small effect on the actual switching time.

In principle, faster switching might be achieved by increasing the field amplitude above the threshold value. However, this can lead to polarity reversal, which reverses the sense of core gyration[4] and can prevent the core from reaching the disk boundary. A fast-moving vortex core loses its rigid character[48] as the kinetic energy is accumulated in the core deformation, and the corresponding effective field, called the gyrofield, can eventually flip the polarity[16,23]. In our case, as the vortex excitation is dominated by the gyrotropic core motion induced by an in-plane spatially homogeneous field, we neglect the contribution of azimuthal spin waves to the core instability[25] and assume the polarity switching occurs when the core velocity v_c reaches a critical value v_{crit} that depends only on the intrinsic parameters of the disk, as predicted by Guslienko *et al.*[23,24].

Simulations show that this becomes an issue for relatively thick and large disks. In the first approximation, assuming a threshold field of $B = B_{\text{an-stat}}/2$, a circular core trajectory (linear regime) and constant ω_0, the maximum core velocity is $\omega_0 R/2$. Considering the pole-free model[5], ω_0 is proportional to L/R and v_c depends only on the disk thickness L. However, ω_0 can be considered constant only during the initial core motion in the linear region[49]. Moreover, as v_c increases with distance between the core and the equilibrium point, it can reach v_{crit} in disks with large R. This

© 2013 Macmillan Publishers Limited. All rights reserved.

possibility is confirmed by simulation of the threshold-field core expulsion in 500/20 and 1,000/20 disks, where the core reaches a velocity above 400 m s^{-1} within the first 30 ps of motion, leading to polarity switching. In 250/20 disks the polarity is conserved and the core is expelled.

However, in our experiments the circulation is switched by pulses in disks up to 30 nm thick and 1,100 nm in diameter. This is not expected based on the analytical model or simulations and can be explained by the positive effect of finite rise time. If the rise time is comparable to the period of the core eigen-oscillation, the core moves together with the equilibrium point (shown schematically in Fig. 3e). The core follows a cycloidal trajectory, and the instantaneous distance between the core and the equilibrium point is decreased, maintaining the core velocity below v_{crit}. Consequently, the amplitude of the pulse has to be increased above $B_{an\text{-}stat}/2$ to expel the core, but the polarity is not flipped.

To gain further insight into vortex annihilation and subsequent circulation switching, time-resolved MTXM using a pump–probe imaging mode[41] was performed. A unipolar field pulse was applied to the sample containing 1,040/20 disks at a repetition rate of 3.05 MHz. It was verified that the magnitude of the pulse was sufficient to switch the spin circulation in the disk. However, in the time-resolved experiment the field polarity was fixed so that the same final circulation was maintained for each imaging cycle. Figure 4a presents stroboscopic images of the vortex annihilation (images 1 to 4, left column) during application of the field pulse plotted in Fig. 4b. The images in the right column of Fig. 4a were produced by micromagnetic simulation, which qualitatively explains the observed magnetic contrast.

The vortex cores follow part of a cycloidal trajectory, because the rise time (4 ns) is comparable to the eigen-oscillation period (5.1 ns for 1,040/20 disks). The symmetric magnetic contrast of the two vortex core trajectories apparent in images 2 to (Fig. 4a) corresponds to two opposite polarities of the vortex core (red and green dots), because the core polarity defines the sense of the core precession[4]. The acquired images represent an average of a multitude of cycles. We conclude that core polarity is not on average conserved during the annihilation–nucleation processes. If vortex core polarity was conserved, the same type of trajectory would be observed for each process. The two core trajectories are schematically illustrated in Fig. 4c. Stroboscopic images of the precession of a vortex core with constant polarity are shown in Supplementary Fig. S3.

In summary, we have experimentally demonstrated controlled spin circulation switching in magnetic vortices with nanosecond field pulses. We further demonstrate that pulsed switching requires approximately half the field strength compared with static switching. The results are supported by both analytical models and micromagnetic simulations, showing that both the time and field switching scales strongly depend on the disk geometry. Importantly, scaling down the disks accelerates circulation switching. The analytical model predicts that switching times shorter than 0.5 ns are possible for 100/20 disks. The limit is set by the transition of the vortex state to a monodomain state for permalloy disks smaller than 100 nm (ref. 50). In Supplementary Movie S1, we present a proof-of-concept simulation of controlled circulation switching in a 100/20 disk with a wedge-like asymmetry. The simulation was carried out using the FastMag finite-element code[51,52].

In our experiments we observe nucleation of a random core polarity upon circulation reversal, preventing full control of vortex chirality by in-plane field pulses. The core polarity could potentially be controlled by an additional out-of-plane bias field[31] or by using pulses with an out-of-plane field component. Alternatively, the core polarity can also be adjusted, as choosing the right geometry of the disks along with the field pulse parameters enables selective polarity switching. Our results present a route to independent control of all four vortex states on subnanosecond timescales.

Methods

Magnetic imaging. Magnetic full-field transmission soft X-ray microscopy (MTXM) experiments were performed at Beamline 6.1.2 at the ALS in Berkeley, California[41]. The spatial resolution of 25 nm was determined by the Fresnel-zone plates used as X-ray objective lenses. Magnetic contrast was obtained using X-ray magnetic circular dichroism (XMCD), giving absorption coefficients proportional to the projection of the magnetization in the direction of the incoming X-rays. The sample was oriented at 60° with respect to the X-ray beam to measure the in-plane magnetization component. Each image was recorded for one circular polarization at the Fe L_3 edge (707 eV).

The contrast was further enhanced by dividing the image by a reference image containing all vortices with the same spin circulation and a reference at saturation. We used both references to unambiguously recognize the circulation switching (Supplementary Fig. S1a–d), as dividing an onion state by a vortex state would result in a contrast that looks like a vortex with spin circulation switched with respect to the reference. We also used subpixel alignment to avoid production of artificial contrast that might be mistaken for circulation switching. For presentation of the results we used a vortex reference for the quasi-static imaging and a reference at saturation for time-resolved imaging. The presented images were processed by band-pass filtering using the ImageJ software to remove spatial frequencies higher than 0.5 px^{-1} (resolution limit) and lower than 0.017 px^{-1} (background removal).

The time-resolved experiments were based on a pump–probe technique enabling stroboscopic imaging of reproducible events[53]. The time structure of the ALS in two-bunch mode operation allowed synchronizing of the field pulses (pump) with the X-ray photon flashes (probe) and recording the temporal evolution of the magnetization in the nanodisks for different delays between the field pulses and photon flashes. The temporal resolution was given by the length of the photon flashes (70 ps) arriving at the sample at 3.05 MHz repetition frequency. The total acquisition time for each image was ~120 s (resp. 480 s, in Supplementary Fig. S3), that is, $\sim 3.7 \times 10^8$ (resp. 1.5×10^9, in Supplementary Fig. S3) events were averaged per single image.

Sample preparation and experimental set-up. Gold-capped permalloy ($Ni_{80}Fe_{20}$) nanodisks with diameters in the range of 250–1,100 nm and thicknesses of 20 and 30 nm were patterned into linear arrays (Fig. 1a) by electron-beam lithography and liftoff processing. The gold capping layer was 2 nm thick. Deposition of the permalloy thin film on a 500-nm-thick polymethyl methacrylate (PMMA) mask was carried out by directional ion-beam sputtering with the sputtered particles incident at 15° from the film normal. Shadowing by the PMMA mask led to a wedge-like asymmetry at one side of the disks (Fig. 1b) with a maximum thickness drop of ~10 nm. The variation of disk thickness was the same in all disks within the sample. Magnetic field pulses were applied by passing a current through a gold waveguide carrying the disks, which was made by liftoff and subsequent trimming to a desired width (0.8–2.2 μm) by a focused ion beam. The entire structure was fabricated on a 200-nm-thick Si_3N_4 membrane to ensure transparency to soft X-rays.

Magnetic field pulses were generated by launching current pulses into the waveguide using a fast pulse generator (Picosecond Pulse Labs 10,050A) with a nominal risetime of 45 ps. The individual pulses were passed through the sample and recorded on a 4 GHz oscilloscope (LeCroy WaveMaster 804Zi-A), allowing the capture of pulse rise times down to 0.1 ns. The recorded rise time was ~0.5 ns, longer than the nominal value due to pulse distortion in the waveguide. Time-resolved experiments were carried out using a different pulser (Agilent 81150A), providing a longer rise time of 2 ns but capable of a repetition rate of 3.05 MHz, which is set by the ALS facility. The recorded pulse shape is shown in Fig. 4b.

The uncertainties of the measurement of pulse amplitude and pulse duration are less than 1% and 5% (standard deviation), respectively. For the determination of switching parameters we used the median of the number of switched disks, with nominal steps of 0.1 ns in the pulse duration and 2 mT in the static field amplitude. The error bars in Fig. 3b correspond to $\pm 1/2$ of this interval combined with the standard deviation of the measurement.

Micromagnetic simulations. Simulations were carried out using the finite-difference code OOMMF[45]. The finite-element code FastMag[51,52] was used for illustration of the circulation switching, including thickness asymmetry (Supplementary Movie S1). The nanodisks were discretized either into cubes with dimensions of $4 \times 4 \times 4$ nm^3 (OOMMF) or into tetrahedrons with a 4 nm mesh size (FastMag). Zero magnetocrystalline anisotropy and an exchange constant of $A_{ex} = 10$ pJ m^{-1} (typical for NiFe) were used. The damping parameter α, spontaneous magnetization M_S and gyromagnetic ratio γ were determined experimentally using ferromagnetic resonance on blanket film samples, with values of $\alpha = 0.0072$, $M_S = 690$ kA m^{-1} and $\gamma = 2.09 \times 10^{11}$ rad Hz T^{-1}. The M_S value was verified by vibrating sample magnetometry.

Received 24 October 2012; accepted 19 March 2013; published online 21 April 2013; corrected online 24 April 2013

References

1. Hubert, A. & Schäfer, R. *Magnetic Domains: The Analysis of Magnetic Nanostructures* (Springer, 1998).

© 2013 Macmillan Publishers Limited. All rights reserved.

2. Shinjo, T., Okuno, T., Hassdorf, R., Shigeto, K. & Ono, T. Magnetic vortex core observation in circular dots of permalloy. *Science* **289,** 930–932 (2000).
3. Wachowiak, A. *et al.* Direct observation of internal spin structure of magnetic vortex cores. *Science* **298,** 577–580 (2002).
4. Choe, S-B. *et al.* Vortex core-driven magnetization dynamics. *Science* **304,** 420–422 (2004).
5. Guslienko, K. Y. *et al.* Eigenfrequencies of vortex state excitations in magnetic submicron-size disks. *J. Appl. Phys.* **91,** 8037–8039 (2002).
6. Novosad, V. *et al.* Spin excitations of magnetic vortices in ferromagnetic nanodots. *Phys. Rev. B* **66,** 052407 (2002).
7. Park, J. P. & Crowell, P. A. Interactions of spin waves with a magnetic vortex. *Phys. Rev. Lett.* **95,** 167201 (2005).
8. Buchanan, K. S., Grimsditch, M., Fradin, F. Y., Bader, S. D. & Novosad, V. Driven dynamic mode splitting of the magnetic vortex translational resonance. *Phys. Rev. Lett.* **99,** 267201 (2007).
9. Antos, R. & Otani, Y. Simulations of the dynamic switching of vortex chirality in magnetic nanodisks by a uniform field pulse. *Phys Rev. B* **80,** 140404(R) (2009).
10. Ishida, T., Kimura, T. & Otani, Y. Current-induced vortex displacement and annihilation in a single permalloy disk. *Phys. Rev. B* **74,** 014424 (2006).
11. Pribiag, V. S. *et al.* Magnetic vortex oscillator driven by d.c. spin-polarized current. *Nature Phys.* **3,** 498–503 (2007).
12. Ruotolo, A. *et al.* Phase-locking of magnetic vortices mediated by antivortices. *Nature Nanotech.* **4,** 528–532 (2009).
13. Kosevich, A. M., Ivanov, B. A. & Kovalev, A. S. Magnetic solitons. *Phys. Rep.* **194,** 117–238 (1990).
14. Van Waeyenberge, B. *et al.* Magnetic vortex core reversal by excitation with short bursts of an alternating field. *Nature* **444,** 461–464 (2006).
15. Lee, K-S. & Kim, S-K. Two circular-rotational eigenmodes and their giant resonance asymmetry in vortex gyrotropic motions in soft magnetic nanodots. *Phys Rev. B* **78,** 014405 (2008).
16. Yamada, K. *et al.* Electrical switching of the vortex core in a magnetic disk. *Nature Mater.* **6,** 269–273 (2007).
17. Bohlens, S. *et al.* Current controlled random-access memory based on magnetic vortex handedness. *Appl. Phys. Lett.* **93,** 142508 (2008).
18. Nakano, K. *et al.* All-electrical operation of magnetic vortex core memory cell. *Appl. Phys. Lett.* **99,** 262505 (2011).
19. Goto, M. *et al.* Electric spectroscopy of vortex states and dynamics in magnetic disks. *Phys. Rev. B* **84,** 064406 (2011).
20. Kikuchi, N. *et al.* Vertical bistable switching of spin vortex in a circular magnetic dot. *J. Appl. Phys.* **90,** 6548–6549 (2001).
21. Hertel, R., Gliga, S., Fähnle, M. & Schneider, C. M. Ultrafast nanomagnetic toggle switching of vortex cores. *Phys. Rev. Lett.* **98,** 117201 (2007).
22. Curcic, M. *et al.* Polarization selective magnetic vortex dynamics and core reversal in rotating magnetic fields. *Phys. Rev. Lett.* **101,** 197204 (2007).
23. Guslienko, K. Y., Lee, K.-S. & Kim, S.-K. Dynamic origin of vortex core switching in soft magnetic nanodots. *Phys. Rev. Lett.* **100,** 027203 (2008).
24. Lee K-S. *et al.* Universal criterion and phase diagram for switching a magnetic vortex core in soft magnetic nanodots. *Phys. Rev. Lett.* **101,** 267206 (2008).
25. Kammerer, M. *et al.* Magnetic vortex core reversal by excitation of spin waves. *Nature Commun.* **2,** 279 (2011).
26. Xiao, Q. F., Rudge, J., Choi, B. C., Hong, Y. K. & Donohoe, G. Dynamics of vortex core switching in ferromagnetic nanodisks. *Appl. Phys. Lett.* **89,** 262507 (2006).
27. Nakano, K. *et al.* Real-time observation of electrical vortex core switching. *Appl. Phys. Lett.* **102,** 072405 (2013).
28. Guslienko, K. Y., Novosad, V., Otani, Y., Shima, H. & Fukamichi, K. Field evolution of magnetic vortex state in ferromagnetic disks. *Appl. Phys. Lett.* **78,** 3848–3850 (2001).
29. Schneider, M., Hoffmann, H. & Zweck, J. Magnetic switching of single vortex permalloy elements. *Appl. Phys. Lett.* **79,** 3113–3115 (2001).
30. Yakata, S., Miyata, M., Nonoguchi, S., Wada, H. & Kimura, T. Control of vortex chirality in regular polygonal nanomagnets using in-plane magnetic field. *Appl. Phys. Lett.* **97,** 222503 (2010).
31. Jaafar, M. *et al.* Control of the chirality and polarity of magnetic vortices in triangular nanodots. *Phys. Rev. B* **81,** 054439 (2010).
32. Mironov, V. L. *et al.* MFM probe control of magnetic vortex chirality in elliptical Co nanoparticles. *J. Magn. Magn. Mater.* **312,** 153–157 (2007).
33. Gaididei, Y., Sheka, D. D. & Mertens, F. G. Controllable switching of vortex chirality in magnetic nanodisks by a field pulse. *Appl. Phys. Lett.* **92,** 012503 (2008).
34. Konoto, M. *et al.* Formation and control of magnetic vortex chirality in patterned micromagnet arrays. *J. Appl. Phys.* **103,** 023904 (2008).
35. Yakata, S. *et al.* Chirality control of magnetic vortex in a square Py dot using current-induced Oersted field. *Appl. Phys. Lett.* **99,** 242507 (2011).
36. Tanase, M. *et al.* Magnetization reversal in circularly exchange-biased ferromagnetic disks. *Phys. Rev. B* **79,** 014436 (2009).
37. Im, M-Y. *et al.* Symmetry breaking in the formation of magnetic vortex states in a permalloy nanodisk. *Nature Commun.* **3,** 983 (2012).
38. Choi, B. C. *et al.* Spin-current pulse induced switching of vortex chirality in permalloy/Cu/Co nanopillars. *Appl. Phys. Lett.* **91,** 022501 (2007).
39. Stoner, E. C. & Wohlfarth, E. P. A mechanism of magnetic hysteresis in heterogeneous alloys. *Phil. Trans. R. Soc. Lond. A* **240,** 599–642 (1948).
40. He, L., Doyle, W. D. & Fujiwara, H. High speed coherent switching below the Stoner–Wohlfarth limit. *IEEE Trans. Magn.* **30,** 4086–4088 (1994).
41. Fischer, P. *et al.* Soft X-ray microscopy of nanomagnetism. *Mater. Today* **9,** 26–33 (January–February, 2006).
42. Cowburn, R. P., Adeyeye, A. O. & Welland, M. E. Controlling magnetic ordering in coupled nanomagnet arrays. *New J. Phys.* **1,** 16 (1999).
43. Natali, M. *et al.* Correlated magnetic vortex chains in mesoscopic cobalt dot arrays. *Phys. Rev. Lett.* **88,** 157203 (2002).
44. Novosad, V. *et al.* Nucleation and annihilation of magnetic vortices in sub-micron permalloy dots. *IEEE Trans. Magn.* **37,** 2088–2090 (2001).
45. Donahue, M. J. & Porter, D. G. *OOMMF User's Guide, Version 1.0*, Interagency Report NISTIR 6376 (National Institute of Standards and Technology, 1999).
46. Cheng, X. M., Buchanan, K. S., Divan, R., Guslienko, K. Y. & Keavney D. J. Nonlinear vortex dynamics and transient domains in ferromagnetic disks. *Phys. Rev. B* **79,** 172411 (2009).
47. Park, J. P., Eames, P., Engebretson, D. M., Berezovsky, J. & Crowell, P. A. Imaging of spin dynamics in closure domain and vortex structures. *Phys. Rev. B* **67,** 020403(R) (2003).
48. Döring, W. On the inertia of walls between Weiss domains. *Z. Naturforsch.* **3a,** 373–379 (1948).
49. Dussaux, A. *et al.* Field dependence of spin-transfer-induced vortex dynamics in the nonlinear regime. *Phys. Rev. B* **86,** 014402 (2012).
50. Chung, S-H., McMichael, R. D., Pierce, D. T. & Unguris, J. Phase diagram of magnetic nanodisks measured by scanning electron microscopy with polarization analysis. *Phys. Rev. B* **81,** 024410 (2010).
51. Chang, R., Li, S., Lubarda, M. V., Livshitz, B. & Lomakin, V. FastMag: fast micromagnetic simulator for complex magnetic structures. *J. Appl. Phys.* **109,** 07D358 (2011).
52. Escobar, M. A. *et al.* Advanced micromagnetic analysis of write head dynamics using FastMag. *IEEE Trans. Magn.* **48,** 1731–1737 (2012).
53. Kasai, S. *et al.* Probing the spin polarization of current by soft X-ray imaging of current-induced magnetic vortex dynamics. *Phys. Rev. Lett.* **101,** 237203 (2008).

Acknowledgements

The authors thank R. Descoteaux and O. Inac for technical help. The authors also thank M. Escobar and V. Lomakin for help with the FastMag simulations, R. Antoš for useful discussions and J. Sapan for editing the manuscript. The research at UCSD was supported by the research programs of the US Department of Energy (DOE), Office of Basic Energy Sciences (award #DE-SC0003678), and the research at CEITEC BUT by the European Regional Development Fund (CEITEC – CZ.1.05/1.1.00/02.0068) and the Grant Agency of the Czech Republic (project no. P102/12/P443). The operation of the X-ray microscope was supported by the Director, Office of Science, Office of Basic Energy Sciences, Materials Sciences and Engineering Division, of the US DOE (contract no. DE-AC02-05-CH11231). Sample nanofabrication was supported by the company TESCAN.

Author contributions

V.U. and M.U. designed and planned the experiment. M.U. and L.H. fabricated the samples. V.U., M.U., J.S. and T.Š. performed the experiments, with help from M-Y.I., P.F., N.E. and J.J.K. V.U. and M.U. carried out the micromagnetic simulations, analysed the data and prepared the figures. E.E.F. was involved in experimental planning and analysis of the results. V.U. wrote the manuscript. All authors commented on the manuscript.

Additional information

Supplementary information is available in the online version of the paper. Reprints and permissions information is available online at www.nature.com/reprints. Correspondence and requests for materials should be addressed to V.U.

Competing financial interests

The authors declare no competing financial interests.

© 2013 Macmillan Publishers Limited. All rights reserved.